Magnetic properties of large area cobalt nanomagnets

2005 J. Phys.: Condens. Matter 17 3931

(http://iopscience.iop.org/0953-8984/17/25/019)

INSTITUTE OF PHYSICS PUBLISHING JOURNAL OF PHYSICS: CONDENSED MATTER

J. Phys.: Condens. Matter **17** (2005) 3931–3941 doi:10.1088/0953-8984/17/25/019

Magnetic properties of large area cobalt nanomagnets

Y S Huang[1], A O Adeyeye[1,3] and N Singh[2]

[1] Information Storage Materials Laboratory, Department of Electrical and Computer Engineering, National University of Singapore, 4 Engineering drive 3, 117576, Singapore
[2] Institute of Microelectronics, 11 Science Park Road, Singapore Science Park II, 117685, Singapore

E-mail: eleaao@nus.edu.sg

Received 17 March 2005, in final form 26 May 2005
Published 10 June 2005
Online at stacks.iop.org/JPhysCM/17/3931

Abstract

We have investigated the magnetization reversal process of cobalt nanomagnetic dot arrays with thickness t in the range from 5 to 90 nm and diameter d in the range from 150 to 250 nm. Large area cobalt nanomagnets were fabricated on Si(100) substrate using deep ultra-violet lithography at 248 nm exposure wavelength. We observed that the magnetic properties of the nanomagnets strongly depend on the thickness and diameter of Co dots due to the effect of the demagnetizing field. The onset of the formation of a magnetization vortex at remanence was found at a phase boundary of thickness and size (e.g., $t = 20$ nm, $d = 250$ nm; $t = 40$ nm, $d = 150$ nm). Above this boundary, vortex annihilation and nucleation fields markedly varied with the thickness and diameter of the dots. Our experimental results are in good agreement with a simple micromagnetic modelling.

(Some figures in this article are in colour only in the electronic version)

1. Introduction

In recent years, magnetic nanostructures have attracted considerable attention due to fundamental research interests and potential applications in data storage and non-volatile magnetic random access memory (MRAM). Research in nanomagnetism has been facilitated by the improvements in controlled nanofabrication techniques such as lithography and other self-assembly methods [1, 2]. From a fundamental viewpoint, an array of identical nanomagnets is a model system for testing various micromagnetics and investigating the magnetization reversal process of nanostructures. From an application viewpoint, nanomagnets form the building blocks for various magnetoelectronic devices such as MRAM and patterned media [3, 4]. A good understanding of the magnetization reversal process is therefore needed in order to design tailor made devices.

[3] Author to whom any correspondence should be addressed.

Great efforts have been devoted to the understanding of the magnetization reversal process of magnetic nanostructures and the magnetization vortex, namely the vortex state, has been discovered in the magnetic switching of ferromagnetic dots [5–8]. When a dot is stable in the vortex state, all the magnetization vectors will circle around one centre and form a vortical configuration. Compared with the single-domain state, the vortex state can significantly reduce the magnetic polarization in a dot and therefore eliminates dipole–dipole interaction between neighbouring dots. Therefore, the vortex state is of great advantage for application in high-density magnetic storage devices.

In this paper, we report on a systematic study of the magnetization reversal of large area Co dot arrays fabricated using deep UV lithography at 248 nm exposure wavelength. The thickness of the Co dots was varied from 5 to 90 nm while the diameter of the dots was varied from 150 to 250 nm. The magnetic properties and the stability of vortex state are strongly dependent on both the thickness and diameter of the Co dots. This may be largely attributed to the effect of demagnetizing field.

2. Experiment details

Large area Co nanomagnets were fabricated on commercially available Si substrate. To create patterns in resist, we coated the substrate with a 60 nm thick anti-reflective layer followed by a 480 nm positive deep ultra-violet (DUV) photoresist. A Nikon lithographic scanner with KrF excimer laser radiation was used to expose the resist. The diameter (d) of the dots was varied from 150 to 250 nm while the pitch of the dot arrays was fixed at 300 nm. Figure 1(a) shows a typical atomic force micrograph (AFM) of the 3D profile of the photoresist layer after exposure and development. This was followed by the electron beam deposition of Cu(20 nm)/Co(t) at a rate of 0.1 Å s^{-1}, in a base pressure of 3.7×10^{-7} Torr. The thickness of the Co layer (t) was varied from 5 to 90 nm. During magnetic film deposition for each thickness, a blank Si(100) wafer was placed in the chamber as a control experiment. Lift-off of the deposited patterned film was carried out in OK73 solution. Completion of the lift-off process was determined by the colour contrast of the patterned area and confirmed by inspection under an atomic force microscope (AFM) and scanning electron microscope (SEM). Shown in figures 1(b) and (c) are the AFM and SEM images of a 20 nm thick Co dot array with a diameter of 250 nm. The nanomagnets are uniform and identical over a large area. Details of the fabrication process are described in our previous work [9].

The magnetization reversal processes in the Co dots were studied using a vibrating sample magnetometer (VSM). In order to investigate the in-plane magnetic behaviour in Co dots, the magnetic field was applied along a fixed direction in the plane of the film as shown in figure 1(c) and swept between −4000 and 4000 Oe at constant rate. All the measurements reported in this paper were conducted at room temperature. The magnetic states in the dot arrays were directly investigated using a magnetic force microscope (MFM).

3. Results and discussion

3.1. Vortex-type switch in a Co dot array

Shown in figure 2(a) is a measured hysteresis loop for an array of 60 nm thick Co dots with diameter $d = 250$ nm. As the applied field is increased from negative saturation, the saturation magnetization is maintained until the applied field is increased to $H_n = -950$ Oe, where a rapid loss of net magnetization occurs. The rapid reduction of net magnetization before the remanence is very characteristic of the nucleation process of a magnetization vortex [10]. As the

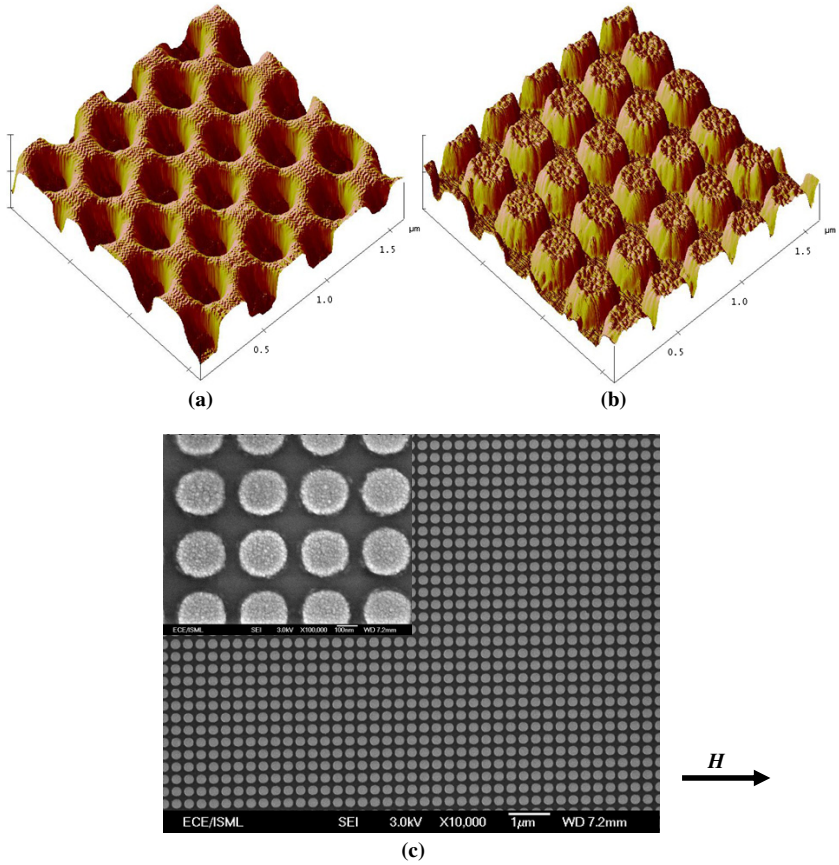

Figure 1. Three-dimensional atomic force micrograph of (a) the photoresist profile after exposure and development and (b) 20 nm thick Co nanomagnetic dots with a diameter of 250 nm and a pitch of 300 nm. (c) Scanning electron microscope (SEM) image of a 20 nm thick Co nanomagnetic dot array. The arrow indicates the direction of the applied field, which is parallel to the rows of dots, during VSM measurements.

applied field is increased beyond $H_1 = -550$ Oe, the magnetization begins to decrease slowly until the magnetization decreases to zero at remanence. The magnetization then increases monotonically as the field is increased from zero to $H_2 = 1200$ Oe. We observed that between H_1 and H_2 the magnetization varies linearly with the applied field and the hysteresis loop is reversible. This behaviour is characteristic of the propagation of the magnetization vortex from one side of the dot to the other. For such a hysteresis loop, the flux closure configuration is formed at remanence, where the magnetization vortex is centred in the dot. This state eliminates the dipole–dipole interaction and lowers the energy of the system by minimizing the magnetostatic energy [5, 10]. As the applied field is further increased beyond H_2, the magnetization increases rapidly until saturation occurs at $H_a = 1500$ Oe, which can be identified as the annihilation process of the magnetization vortex. The switching field H_n, which indicates the onset of vortex nucleation, is known as the nucleation field, while the saturation field H_a, which indicates the termination of vortex annihilation, is termed the annihilation field. The fast but non-abrupt nucleation and annihilation process in figure 2(a) is attributed to the distribution of nucleation and annihilation fields in the dot array [5].

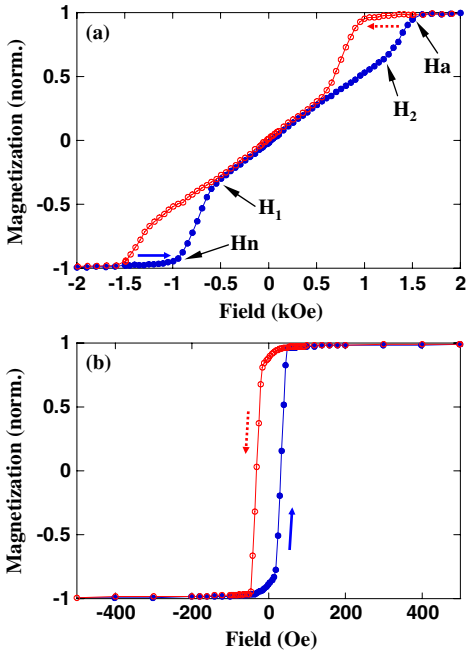

Figure 2. Hysteresis loops from (a) a 60 nm thick Co nanomagnetic dot array and (b) a 60 nm thick reference film for fields applied along the in-plane easy axis.

Also shown in figure 2(b) is a hysteresis loop for the reference film deposited under the same conditions. The reference film shows a quasi-rectangular hysteresis loop with a coercivity of 32 Oe and a squareness (M_r/M_s) of 0.88. We observed that both the switching field and detailed features of the loop are different from the Co dot array in figure 2(a). The magnetic behaviour in Co dots can thus be attributed to the effect of the demagnetizing field. The dots have much larger in-plane demagnetizing factor than the reference film due to smaller lateral size [11]. Hence, the dots feel larger in-plane demagnetizing field at saturation and tend to switch more easily compared with the reference film. Meanwhile, the vortex state is formed to decrease the magnetostatic energy in Co dots.

In order to confirm the exact magnetic state in the dot array at remanence, we have performed magnetic force microscopy (MFM) measurements. Before the image was taken, a field of 3000 Oe was applied in the plane of the sample to saturate the Co dots. Then the applied field was decreased gradually to zero so that the quasi-static magnetization reversal occurred in the Co dots. A magnetized Si tip coated with CoCr was used to scan the MFM image of the dot array at the remanence state. Shown in figure 3 is the MFM image of a 60 nm thick Co dot array. The light and the dark spots at the centre of the dots correspond to the vortex cores with up and down magnetization respectively, which are formed to lower the strong exchange energy at the centre of the magnetization vortex [12, 13]. The mixture of the light and the dark spots at the centre of the dots in the MFM image shows that the orientations of the vortex cores are random when only the in-plane field is present during the magnetization reversal process.

3.2. Thickness dependent vortex-type magnetization reversal

In order to further investigate the vortex-type magnetization reversal in Co dot arrays, we carried out a systematic study of the effect of Co dot thickness. The dot diameter was fixed at 250 nm

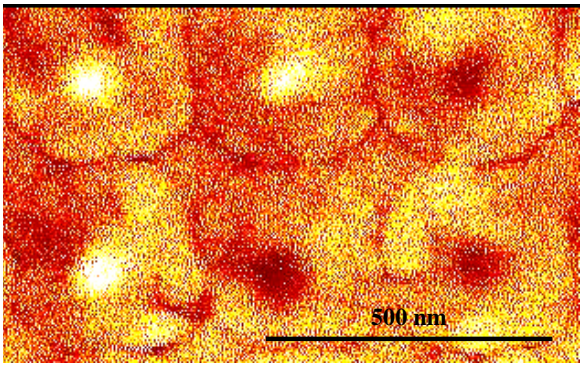

Figure 3. Magnetic force micrograph of a 60 nm thick Co nanomagnetic dots with a diameter of 250 nm and a pitch of 300 nm as the applied field is reduced from positive saturation field to zero. A typical magnetization vortex can be observed from the MFM image. The light and the dark spots at the centre of the dots correspond to the vortex cores with up and down magnetization respectively.

while the Co thickness was varied from 5 to 90 nm. Shown in figure 4 is the representative hysteresis loops from the Co dots as a function of thickness (t). For $t < 20$ nm, typical single-domain switching can be observed from the hysteresis loop. For $t = 20$ nm, the rapid reduction of magnetization around zero field indicates the onset of vortex-type magnetization reversal, where the nucleation field is -150 Oe and the annihilation field is 800 Oe. However, unlike the typical vortex hysteresis loop shown in figure 2(a), the nucleation process terminates after the remanence state and therefore the remanent magnetization is non-zero. We believe that the vortex state and the buckling state, c or s states in most cases [8], may co-exist in the Co dot array at remanence. As the Co thickness t is increased to 30 nm, a typical vortex hysteresis loop is observed, where the nucleation process terminates before the remanence and the remanent magnetization is decreased to zero, indicating that all the Co dots in the array form the flux closure configuration. Furthermore, the nucleation field is decreased to -260 Oe while the annihilation field is increased to 950 Oe. Upon increasing the Co thickness from 30 to 90 nm, the annihilation field increases from 950 to 1800 Oe while the nucleation field decreases from -260 to -1500 Oe. Meanwhile, the gradients of vortex nucleation and annihilation parts of the loop are decreased, indicating the increase of the distributions of nucleation and annihilation fields with the thickness. In addition, the linear and reversible region of the loop, which corresponds to vortex propagation, extends with the thickness, indicating that thicker Co dots tend to remain stable in a vortex state over a wider field range.

3.3. Size dependent vortex-type magnetization reversal

Similar evolution of the vortex-type hysteresis behaviour with the lateral size of the dot was also studied. In this case, the diameter of the dots (d) was varied from 150 to 250 nm while the thickness was fixed at 40 nm. Shown in figure 5 is the evolution of the hysteresis loops as a function of Co dot diameter. A vortex-type magnetization reversal process can be observed at each diameter. As the diameter is decreased from 250 to 150 nm, the nucleation field decreases from -500 to -700 Oe while the annihilation field increases from 1250 to 1600 Oe respectively. On the other hand, the distributions of the nucleation and annihilation fields are increased and the region of vortex propagation is markedly sensitive to Co dot diameter. We also observed that Co dots with smaller diameter will remain in a vortex state over a wider field range.

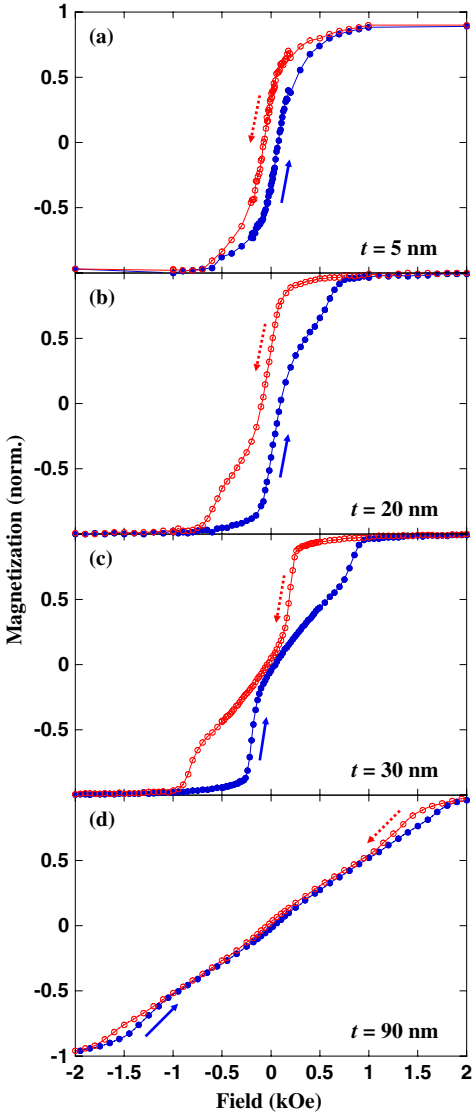

Figure 4. Representative magnetic hysteresis loops for Co dot arrays as a function of Co thickness for diameter $d = 250$ nm.

Similar to the vortex-type hysteresis loop for $d = 250$ nm and $t = 20$ nm (figure 4(b)), the hysteresis loop for $d = 150$ nm and $t = 40$ nm displayed in figure 5(a) also shows a non-zero remanent magnetization. However, this remanent magnetization cannot be attributed to the presence of a buckling state at zero field, because the nucleation process terminates before the remanence state. Instead, it may be due to the co-existence of both the vortex-type magnetization reversal and single-domain switching in the dot array. This has been verified by taking the MFM image at remanence after applying a large field and then reducing the field to zero. Shown in figure 6(a) is an MFM image for a $d = 150$ nm and $t = 40$ nm dot array at remanence. A mixture of both the flux closure and single-domain configurations

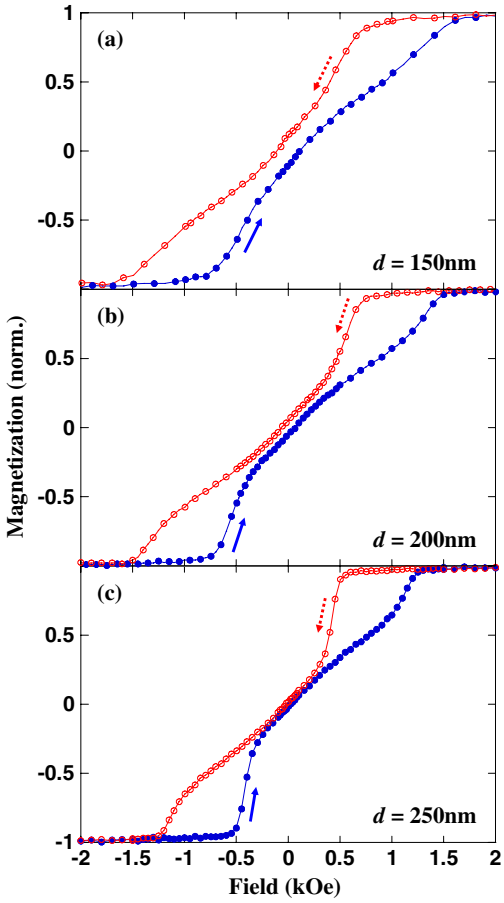

Figure 5. Representative magnetic hysteresis loops for Co dot arrays as a function of the diameter of the dots for thickness $t = 40$ nm.

can be observed from figure 6(a). The dots with a dark or light spot at the centre indicate the flux closure configuration, where the magnetization vectors at the edge form a vortical configuration in the plane and those at the centre orient perpendicular to the plane. The dots with sharp contrast between two sides, on the other hand, indicate the single-domain configuration, where the magnetization is uniform. There is thus a good agreement with our interpretation of the hysteresis loops. We also observed that the remanent magnetization decreases with the size of the dots, indicating the gradual extinction of the single-domain switch in the array. For $d = 250$ nm and $t = 40$ nm, the remanent magnetization decreases to zero, indicating that only the flux closure configuration is present. This has also been confirmed using magnetic force microscopy (figure 6(b)).

It has been reported by Cowburn *et al* [10] that for permalloy nanomagnets the single-domain switching in a dot array will be replaced by the vortex-type magnetization reversal above a phase boundary of thickness and size. This is in good agreement with our experimental results for Co nanomagnets. In addition, we found non-zero remanent magnetization in the vortex-type hysteresis behaviour at the phase boundary, which was due to the presence of buckling states or a single-domain state at remanence.

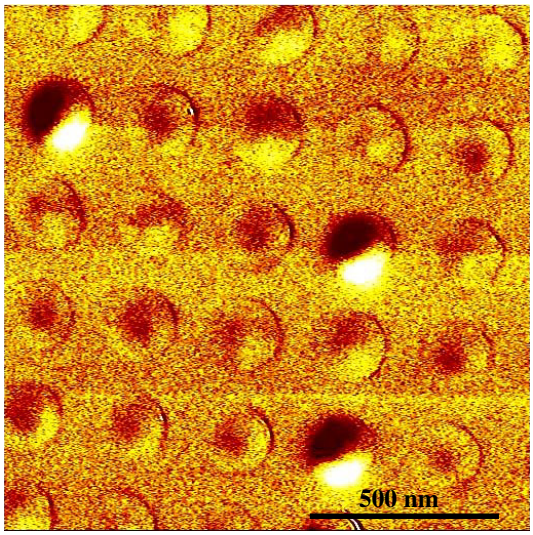

(a)

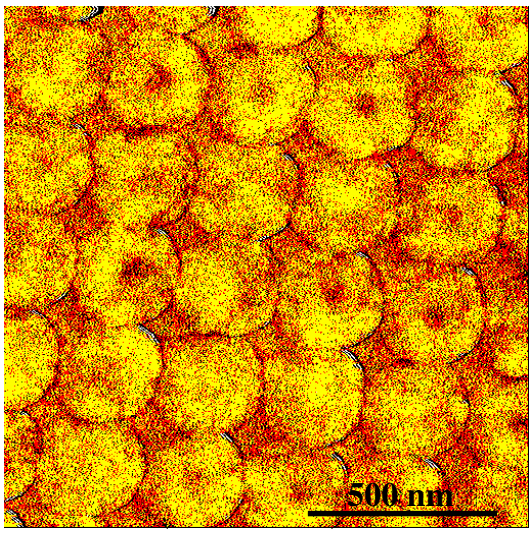

(b)

Figure 6. Magnetic force micrographs of 40 nm thick Co dots with the diameters of (a) 150 nm and (b) 250 nm at remanence after applying a saturation field. The dots with a dark or light spot at the centre indicate the flux closure configuration. The dots with strong contrast between two sides indicate the single-domain configuration. For $d = 150$ nm a mixture of flux closure and single-domain configurations can be observed, while for $d = 250$ nm only the flux closure configuration can be seen.

3.4. Modelling of vortex nucleation and annihilation

To understand the physics behind the vortex-type magnetization reversal in Co dots, we simulated the nucleation and annihilation process using the 'rigid' vortex model proposed by Guslienko *et al* [6], where the magnetization reversal in a soft ferromagnetic dot is interpreted as the shift of an unalterable magnetization vortex. The magnetization distribution for a shifted

magnetization vortex can be expressed in complex coordinates as [14]

$$m_x + \mathrm{i}m_y = \frac{2w}{1+w\bar{w}}, \qquad m_z = \frac{1-w\bar{w}}{1+w\bar{w}}$$
$$w = \begin{cases} f(\zeta) & |f(\zeta)| < 1 \\ f(\zeta)/|f(\zeta)| & |f(\zeta)| \geqslant 1 \end{cases}, \qquad \zeta = x + \mathrm{i}y. \tag{1}$$

In the 'rigid' vortex model, the field is applied along the x-axis and the vortex core moves along the y-axis, hence we obtain $f(\zeta) = (\mathrm{i}/c)(\zeta - \mathrm{i}a)$, where $a = \Delta/R$ is the relative core displacement and $c = R_{\mathrm{core}}/R$ is the relative centred core radius [15] (Δ, R and R_{core} are core displacement, dot radius and core radius). During the annihilation process, the vortex core shifts inside the dot ($|a| < 1 - c$). Taking account of the magnetization distribution in equation (1), the exchange energy density is written as

$$e_{\mathrm{ex}}(a) = \frac{E_{\mathrm{ex}}}{V} = \frac{A}{V}\int_V \sum_{i,j=1}^{3} (\nabla_i m_j)^2 \,\mathrm{d}\tau$$
$$= \frac{2A}{R^2}\left(2 - \ln\frac{c}{1-a}\right) + \frac{2A}{\pi R^2}\int_{1-a}^{1+a} \frac{\mathrm{d}\rho}{\rho} \arccos\frac{a^2+\rho^2-1}{2a\rho}. \tag{2}$$

In order to model cobalt dots, we modified Guslienko's model by incorporating the magnetocrystalline anisotropy energy. In a uniaxial anisotropic crystal like hcp cobalt, the anisotropy energy density for magnetization vortex is expressed as

$$e_{\mathrm{an}} = \frac{1}{V}\int K_{\mathrm{u}}[1 - (\vec{m}\cdot\vec{u})^2]\,\mathrm{d}\tau = \frac{K_{\mathrm{u}}}{\pi}\int_{1-a}^{1+a} \mathrm{d}\rho \int_{-\arccos\frac{a^2+\rho^2-1}{2a\rho}}^{\arccos\frac{a^2+\rho^2-1}{2a\rho}} [1 - \sin^2\theta_{\mathrm{u}}\cos^2(\varphi - \varphi_{\mathrm{u}})]\rho\,\mathrm{d}\varphi$$
$$+ \frac{K_{\mathrm{u}}}{2}[(4\ln 2 - 3)(3\cos^2\theta_{\mathrm{u}} - 1)c^2 + (1 + \cos^2\theta_{\mathrm{u}})(1-a)^2] \tag{3}$$

where $\vec{u}(\theta_{\mathrm{u}}, \varphi_{\mathrm{u}})$ is the unit vector of the c-axis in spherical coordinates and K_{u} is the uniaxial magnetocrystalline anisotropy constant. The total energy density is thus expressed as a function of relative core displacement a and external field H

$$e_{\mathrm{vo}}(a, H) = e_{\mathrm{ex}}(a) + e_{\mathrm{an}}(a) + e_{\mathrm{ms}}(a) + e_{\mathrm{H}}(a, H) \tag{4}$$

where $e_{\mathrm{H}}(a, H) = -HM_x(a)$ is the Zeeman energy and $e_{\mathrm{ms}}(a) = 2\pi M_{\mathrm{s}}^2 F_1^V(1/r)a^2$ is the magnetostatic energy [6]. The annihilation field H_{a}, beyond which the core shifts out of the dot, is thus obtained by solving $\partial e_{\mathrm{vo}}(a, H_{\mathrm{a}})/\partial a|_{a=1-c} = 0$

$$H_a = \frac{\mathrm{d}(e_{\mathrm{an}} + e_{\mathrm{ex}})/\mathrm{d}a|_{1-c} + 4\pi M_{\mathrm{s}}^2(1-c)F_1^V(1/r)}{\mathrm{d}M_x/\mathrm{d}a|_{1-c}}$$
$$F_\mu^V(1/r) = \int_0^\infty \frac{1}{p}\left[1 - \frac{r(1-\mathrm{e}^{-p/r})}{p}\right] J_\mu^2(p)\,\mathrm{d}p \tag{5}$$
$$M_x(a) = M_{\mathrm{s}}a\left[\frac{2}{\pi}K(a^2) - \frac{3}{8}a^2\,{}_2F_1\left(\frac{1}{2}, \frac{5}{2}; 3; a^2\right)\right]$$

where $r = R/t$ is the aspect ratio, $J_\mu(x)$ is the Bessel function, $K(x)$ is the complete elliptic integral of the first kind and ${}_2F_1(x, y; z; b)$ is the Gauss hypergeometric function.

During the nucleation process, the magnetization vortex is assumed to shift from infinite to the dot. Near negative saturation, the total energy density of the uniaxial anisotropic crystal is expressed as

$$e_{\mathrm{sd}}(\theta, H) \simeq K_{\mathrm{u}}(1 - \sin^2\theta_{\mathrm{u}}\cos^2\varphi_{\mathrm{u}}) - \frac{2A\ln(\cos\theta)}{R^2} + NM_{\mathrm{s}}^2/2$$
$$+ HM_{\mathrm{s}} + \left\{\frac{K_{\mathrm{u}}\sin^2\theta_{\mathrm{u}}\cos 2\varphi_{\mathrm{u}}}{2} - \frac{HM_{\mathrm{s}}}{8} - \frac{\pi M_{\mathrm{s}}^2 F_2^V(1/r)}{2}\right\}\theta^2 \tag{6}$$

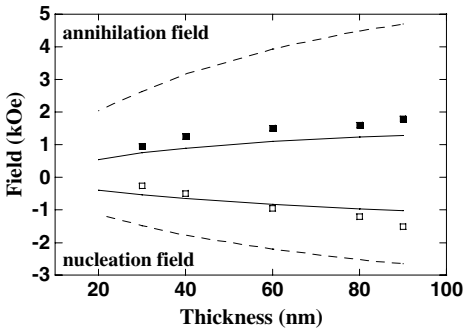

Figure 7. The simulated and measured annihilation field H_a and nucleation field H_n for Co dot arrays as a function of thickness when the diameter is fixed at 250 nm. The dashed lines (single dot) and the solid lines (coupled dots) are simulated using the 'rigid' vortex model. The solid and hollow squares represent the experimental annihilation and nucleation field, respectively.

where θ satisfies $\sin\theta = 1/a \simeq 0$ and N is the in-plane demagnetization coefficient [11]. The vortex nucleation occurs when the uniform magnetization is unstable. That is,

$$\begin{aligned} &\partial e_{sd}(\theta, H)/\partial\theta = 0 \\ &\partial^2 e_{sd}(\theta, H)/\partial\theta^2 = 0. \end{aligned} \tag{7}$$

The nucleation field is thus obtained.

$$H_n = \frac{8A}{R^2 M_s} + \frac{4K_u \sin^2\theta_u \cos 2\varphi_u}{M_s} - 4\pi M_s F_2^V(1/r). \tag{8}$$

The annihilation and nucleation fields for a single dot have been given by equations (5) and (8). When the dot pitch T is comparable with diameter d in a square array, the inter-dot coupling becomes significant. Hence, inter-dot coupling should be involved in the magnetostatic energy. In such a case, $F_\mu^V(1/r)$ in equation (5) should be rewritten as [16]

$$\begin{aligned} F_\mu^V(1/r) &= \frac{1}{\pi}\sum_{i,j=0}^{\infty}\left[1 - \frac{r(1-e^{-p/r})}{p}\right]\left[\frac{J_\mu(p)i}{i^2+j^2}\right]^2 \\ p &= 2\pi R\sqrt{i^2+j^2}/T. \end{aligned} \tag{9}$$

In our modelling, we assumed that the in-plane shape anisotropy was negligible, which agreed with our experimental results. Figure 7 shows the simulated and measured nucleation field H_n and annihilation field H_a as a function of thickness when the diameter is fixed at 250 nm. The dashed lines show the modelling H_a and H_n for a single Co dot while the solid lines show the modelling H_a and H_n for coupled Co dots with a pitch of 300 nm. We noticed that the absolute values of both the nucleation and annihilation fields decrease significantly when the effect of inter-dot coupling is involved. This implies that the inter-dot coupling caused by the stray field will weaken the stability of the vortex state. The corresponding experimental data are illustrated in figure 7 using solid square symbols (annihilation field) and hollow square symbols (nucleation field). There is a very good agreement between the theoretical modelling for coupled Co dots and our experimental measurement. When examining equations (5) and (8), it is found that the magnetostatic energy related terms are dependent on the aspect ratio r and the exchange energy related terms are functions of the size of the dot. The anisotropy energy related terms, however, are independent of the size and thickness. Therefore, the thickness dependent nucleation and annihilation result from the magnetostatic energy. The size dependent nucleation and annihilation are attributed to the exchange energy as well as

the magnetostatic energy. Further examining equations (5) and (8), we noticed that for small aspect ratio ($r < 10$) and large size ($R > 100$ nm) the magnetostatic energy has a much larger effect on vortex nucleation and annihilation in Co dots than the exchange energy, whereas for small size ($R < 10$ nm) the effect of magnetostatic energy is negligible compared with that of exchange energy.

4. Conclusions

We have fabricated Co nanomagnetic dot arrays of different thicknesses using DUV lithography at 248 nm wavelength. We observed that the magnetic properties and the reversal mechanism in the Co nanodots strongly depend on the thickness and diameter of Co dots. The onset of the formation of the vortex state was observed at a phase boundary of size and thickness. The vortex nucleation and annihilation has been explained using a modified 'rigid' vortex model. Our experimental results agree well with theoretical simulation incorporating inter-dot coupling.

Acknowledgments

This work was supported by the National University of Singapore (NUS) grant No R263-000-283-112. One of the authors (YSH) is supported by an NUS research scholarship.

References

[1] Smyth J F, Schultz S, Fredkin D R, Kern D P, Rishton S A, Schmid H, Cali M and Koehler T R 1991 *J. Appl. Phys.* **69** 5262
[2] Adeyeye A O, Bland J A C, Daboo C, Hasko D G and Ahmed H 1997 *J. Appl. Phys.* **82** 469
[3] Daughton J M 1998 *J. Magn. Magn. Mater.* **192** 334
[4] Zhu J G and Zheng Y 1998 *IEEE Trans. Magn.* **34** 1063
[5] Lebib A, Li S P, Natail M and Chen Y 2001 *J. Appl. Phys.* **89** 3892
[6] Guslienko K Y, Novosad V, Otani Y, Shima H and Fukamichi K 2001 *Phys. Rev.* B **65** 024414
[7] Prejbeanu I L, Natali M, Buda L D, Ebels U, Lebib A, Chen Y and Ounadjela K 2002 *J. Appl. Phys.* **91** 7343
[8] Rahm M, Schneider M, Biberger J, Pulwey R, Zweck J, Weiss D and Umansky V 2003 *Appl. Phys. Lett.* **82** 4110
[9] Singh N, Goolaup S and Adeyeye A O 2004 *Nanotechnology* **15** 1539
[10] Cowburn R P, Koltsov D K, Adeyeye A O, Welland M E and Tricker D M 1999 *Phys. Rev. Lett.* **83** 1042
[11] Osborn J A 1945 *Phys. Rev.* **67** 351
[12] Sinhjo T, Okuno T, Hassdorf R, Shigeto K and Ono T 2000 *Science* **15** 930
[13] Raabe J, Pulway R, Sattler R, Schweinbock T, Zweck J and Weiss D 2000 *J. Appl. Phys.* **88** 4437
[14] Metlov K L 2000 *Preprint* cond-mat 0012146v1
[15] Usov N A and Peschany S E 1993 *J. Magn. Magn. Mater.* **118** L290
[16] Guslienko K Y 1999 *Appl. Phys. Lett.* **75** 394